

Article

Intra-Molecular Electrical Field Regulated Nonlinear Catalyst Charge Transfer in the Organic Conjugated Molecular System

Quanjiang Li ¹, Shenghui Chen ^{1,*}, Li Wang ¹, Yanli Liu ¹, Di He ¹, Meishan Wang ^{2,*}  and Jingang Wang ³ 

¹ School of Physics and Optoelectronics Engineering, Ludong University, Yantai 264025, China; lqj@ldu.edu.cn (Q.L.); wangl@ldu.edu.cn (L.W.); yanliliu@ldu.edu.cn (Y.L.); hedi@ldu.edu.cn (D.H.)

² School of Integrated Circuits, Ludong University, Yantai 264025, China

³ College of Science, Liaoning Petrochemical University, Fushun 113001, China; jingang_wang@lnpu.edu.cn

* Correspondence: csh2010@163.com (S.C.); mswang1971@163.com (M.W.)

Abstract: The application of organic conjugated molecular systems to photocatalysis is based on the charge transition with different electronegative substituents and the electron-hole separation behavior of charge transfer under light excitation. In this work, the relationship between the intra-molecular electrical field and molecular second-order nonlinear optical properties is investigated theoretically by the sum-of-states (SOS) method. We use substituents with different electron affinity energy to construct internal electric fields with different properties in similar conjugated systems. The studies of these systems reveal the intra-molecular electric field strength and mode regulation of nonlinear optical coefficients and explain its physical mechanism. The intra-molecular charge recombination caused by the electrostatic potential multipole field of different substituents changes the transition behavior of one-photon, resulting in the enhancement of nonlinear optical properties (second-harmonic generation and sum-frequency coefficient) greater than 10^4 .

Keywords: intra-molecular electrical field; second-order nonlinear optical; conjugated molecular system; sum-of-state; electrostatic potential multipole field



Citation: Li, Q.; Chen, S.; Wang, L.; Liu, Y.; He, D.; Wang, M.; Wang, J. Intra-Molecular Electrical Field Regulated Nonlinear Catalyst Charge Transfer in the Organic Conjugated Molecular System. *Catalysts* **2021**, *11*, 1375. <https://doi.org/10.3390/catal11111375>

Academic Editors: Detlef W. Bahnemann, Ewa Kowalska, Ioannis Konstantinou, Magdalena Janus, Vincenzo Vaiano, Wonyong Choi and Zhi Jiang

Received: 22 October 2021
Accepted: 13 November 2021
Published: 15 November 2021

Publisher's Note: MDPI stays neutral with regard to jurisdictional claims in published maps and institutional affiliations.



Copyright: © 2021 by the authors. Licensee MDPI, Basel, Switzerland. This article is an open access article distributed under the terms and conditions of the Creative Commons Attribution (CC BY) license (<https://creativecommons.org/licenses/by/4.0/>).

1. Introduction

In recent years, organic molecules with conjugated systems have been widely used in many electronic devices [1–4]. In perovskite solar cells (PSCs) [5–8], stability can be increased. In dye-sensitized solar cells (DSSCs) [9–12], the conjugate system is a good electron transport material [13–15]. Moreover, the widely used two-dimensional material graphene [16–22] also has a wide range of conjugated systems. A common feature of these applications is that electrons are strongly delocalized in conjugated systems and can provide high electron mobility [21–23]. Therefore, the excellent properties of conjugated systems have potential in the fields of electricity and optics. However, the performance requirements of applications in different fields are varied. Therefore, in specific application scenarios, researchers will make various chemical modifications to these conjugated molecules or materials. It is embodied in the modification of different functional groups, which can significantly improve the performance of the material. In the field of optics, different functional groups can significantly affect the photon-induced charge-transfer (PICT) properties of the system by improving the natural bond orbits (NBO) and natural transition orbits (NTO) [24].

In fact, the modification of the optical properties of the system by different functional group modifications does not stop there. Different functional groups also have a great influence on nonlinear optical properties. This is because the introduction of functional groups changes the electric field distribution in the molecule or the system, which causes a large change in the molecular dipole moment or fragment dipole moment, causing a change in the nonlinear optical properties. This is because the nonlinear optical properties are theoretically defined by the sum-of-state (SOS) [25,26] of the system dipole moment

and transition dipole moment. In other words, the functional group controls the nonlinear optical parameters of the molecule by changing the dipole electric field and the multipolar electric field in the molecule. Therefore, it can also be said that it is the nonlinear optical property which is controlled by the electric field in the molecule. In this work, we used different functional groups and the same conjugated core combination to explore the ability of this intra-molecular electric field to control the nonlinear optical properties, especially the second-order nonlinear optical properties. In addition, through theoretical calculations, we reveal the physical mechanism of this regulation. This mechanism will be beneficial to nonlinear optical microscopes, especially second-harmonic generation (SHG) microscopes, which provide new theoretical guidance to the performance of the electronic devices described above.

2. Results and Discussion

2.1. Molecular Structure, Linear and Nonlinear Optical Properties

In this theoretical work, we chose a molecular system with a strong conjugated anthracene and carbon–carbon triple bond as the core, see Figure 1. This part of the conjugate center can serve as a bridge for electron transmission. However, different electronegative substituents are used at both ends of the conjugate core. These substituents can provide different push–pull functions for electrons. In fact, the electronic push–pull properties are determined by the electrostatic forces in the four basic interactions. Therefore, in combination with conjugated cores and substituents, intra-molecular electric fields of different sizes and directions will be formed in the molecule, and this internal electric field will have a regulatory effect on the nature of the electron transition.

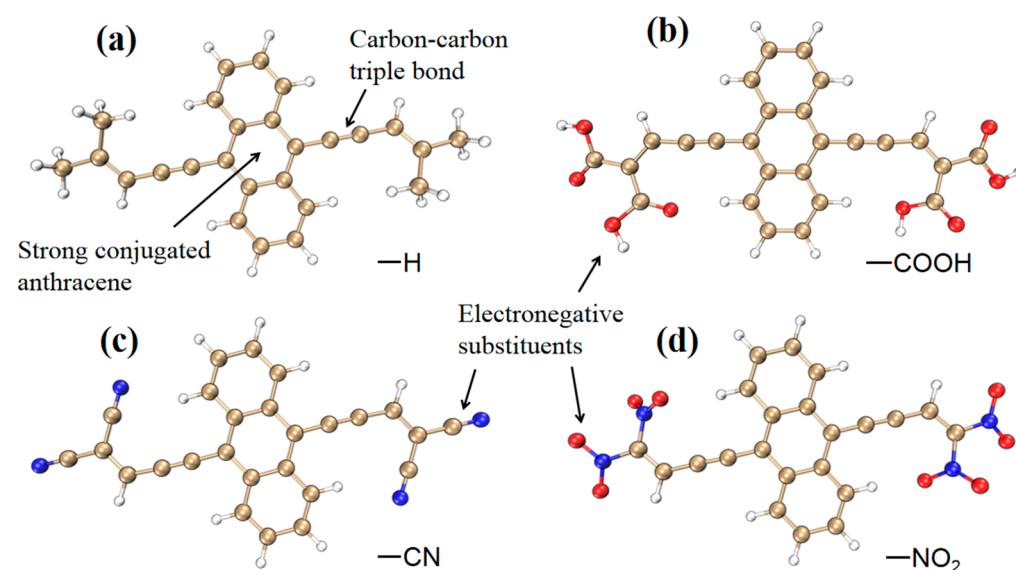


Figure 1. The optimized molecular geometry structures of different substituent group conjugated systems of -H (a), -COOH (b), -CN (c) and -NO₂ (d).

The transition energy of electrons is reflected in the position of the absorption peak in the absorption spectrum. As shown in Figure 2a, the excitation energy of the absorption spectrum of different substituent molecular systems is hugely different. When there is no substituent, this is the case when H is used as a substituent. Its absorption peak is around 450 nm. When replaced with other substituents, the peak position of the absorption spectrum has a red shift, that is, it moves to a long wavelength. In addition, the degree of red shift is different due to different substituents. Among them, the absorption peak wavelength with nitro group has the longest wavelength (560 nm). This is due to the inconsistent potentials of different substituents. The same nature will be reflected in the frequency doubling effect. As shown in Figure 2b, the dynamic second-harmonic generation coefficients with different substituents are shown. First, referring to Figure 2a,

it can be found that the wavelength corresponding to the strongest SHG coefficient strictly corresponds to the absorption spectrum peak of the first excited state. This is because the intensity of the absorption spectrum is determined by the oscillator strength, and the oscillator strength (f) is defined as:

$$f = \frac{2}{3} \Delta\varepsilon \langle j | \mu | i \rangle \quad (1)$$

where the $\Delta\varepsilon$ is the excited energy and the $\langle j | \mu | i \rangle$ is the transition dipole moment. Therefore, the system with higher transition dipole moment will also have a larger SHG coefficient. On the other hand, the SHG coefficients of molecular systems with different substituents are hugely different. The highest SHG of the cyano system is only 10^3 and the SHG coefficient of the carboxyl system is as high as 10^7 , which differs by four orders of magnitude. The SHG of H system and nitro system both reached 10^5 . This shows that different substituents have a great degree of regulation on the SHG coefficient.

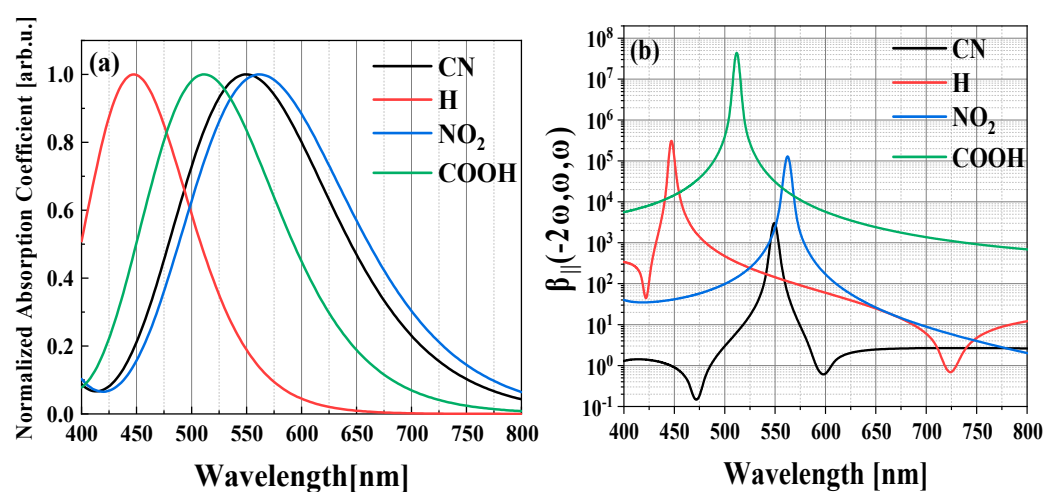


Figure 2. The one-photon absorption spectra (a), frequency-dependent second-harmonic generation coefficient spectra (b).

Relative to the SHG coefficient, the sum-frequency coefficient is also controlled by substituents and has the same properties. As shown in Figure 3, the sum-frequency coefficients of different substituent molecular systems are shown. First, the coordinate axis in the figure represents the wavelength of the incident light and the color bar represents the magnitude of the sum-frequency coefficient. The diagonal is the frequency multiplication factor. Second, the regions with relatively large sum-frequency coefficients constitute concentric elliptical rings, while the number of elliptical rings of different substituent molecular systems is different. Third, because the range of the color bars in the figure is the same, it can be intuitively found that the carboxyl system has a high sum-frequency coefficient and the cyano system is the lowest.

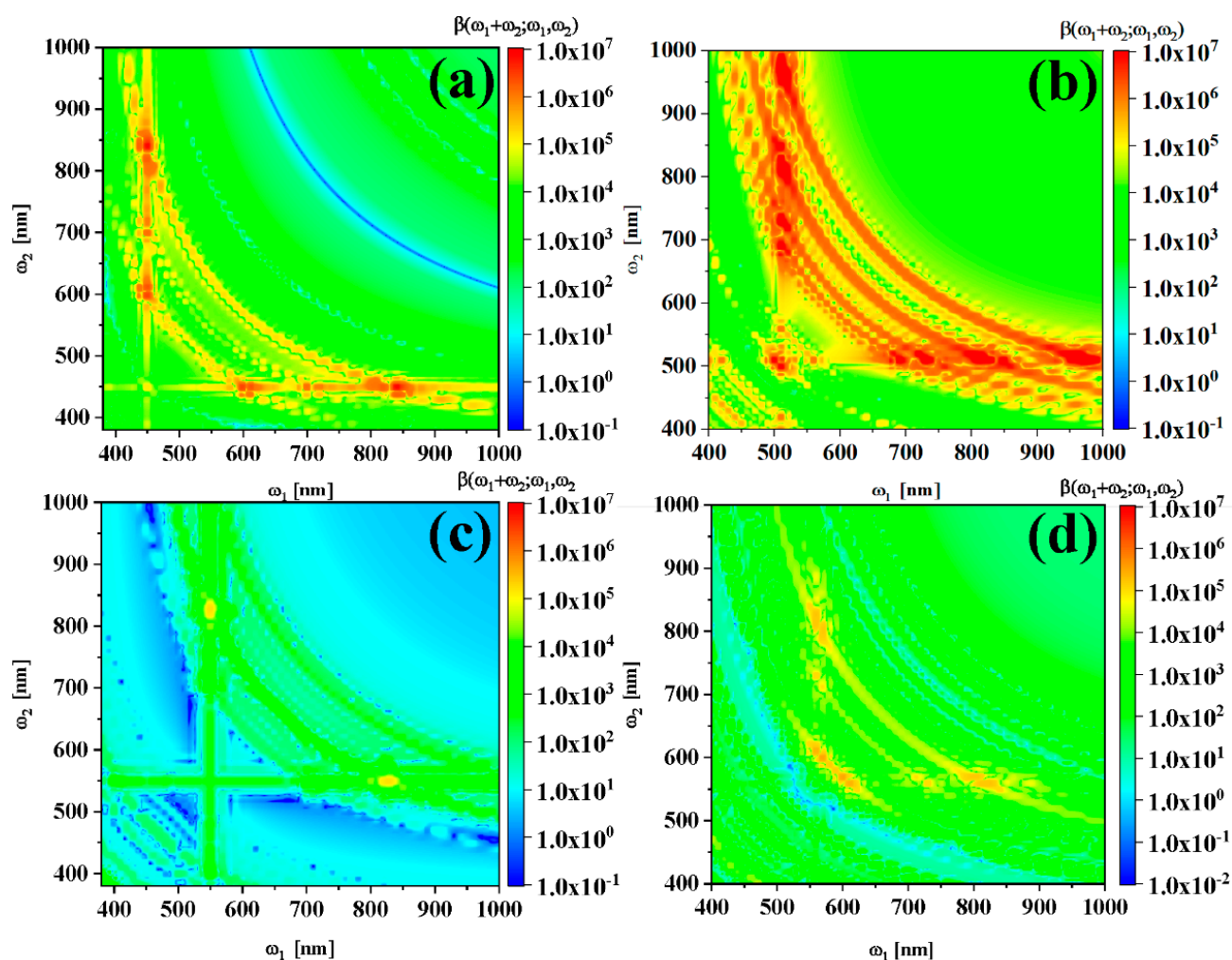


Figure 3. The sum-frequency coefficients of -H (a), -COOH (b), -CN (c) and -NO₂ (d) conjugated molecular systems.

2.2. Physical Mechanism and Transition Characteristic

In order to explore the physical mechanism of the regulatory effect of substituents on molecular systems, we first visually studied the transition characteristics of the first excited state. As shown in Figure 4, it is the electron-hole pair density analysis and transition density matrix diagram of the first excited state of different substituent molecular systems. It can be seen intuitively from the figure that the charge-transfer characteristics is in the transition process. As shown in Figure 4a, it is the transition characteristics of the molecular system without substituents. The separation of electrons and holes is not obvious, indicating a localized excitation. Conversely, the molecular system containing substituents has a high degree of separation between electrons and holes, which shows obvious charge-transfer characteristics, see Figure 4b,c. In addition, the hole density of the carboxyl system and the cyano system is on the conjugated ring, and the electron density is distributed on the substituent, indicating the charge transfer from the conjugated system to the substituent. Different from this, the hole density of the nitro system is distributed on the nitro group and the electron density is distributed on the conjugated ring, indicating that the charge transfer is excited from the nitro group to anthracene, see Figure 4d.

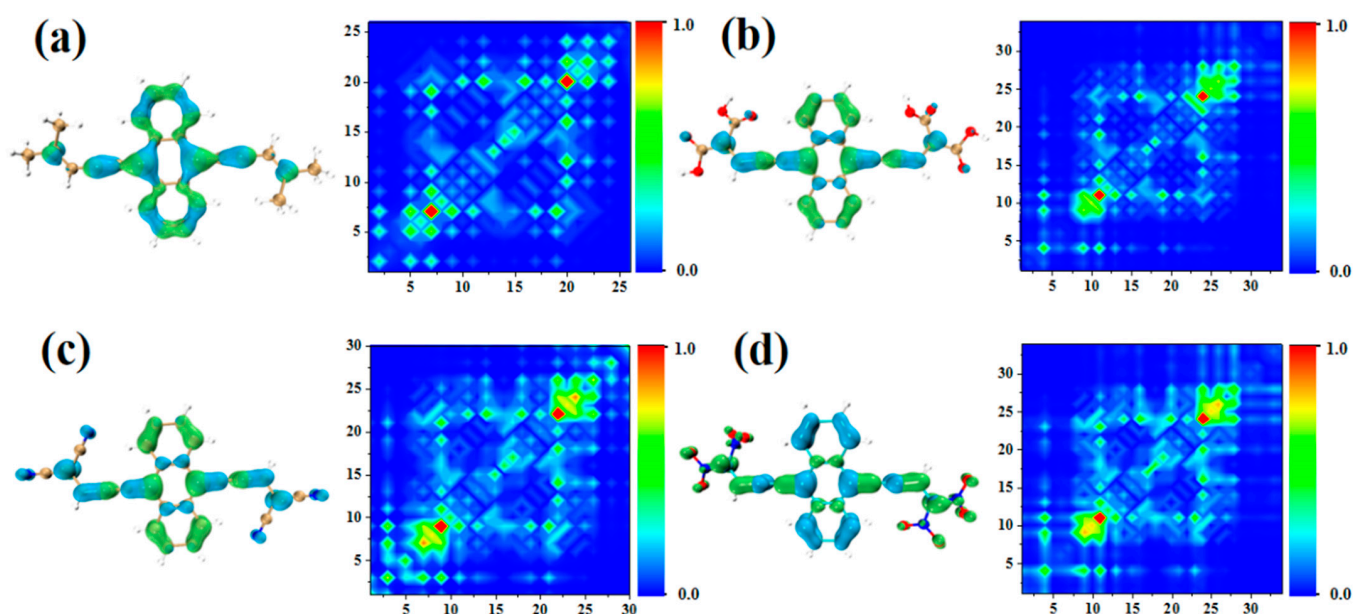


Figure 4. The one-photon absorption transition characteristics of -H (a), -COOH (b), -CN (c) and -NO₂ (d) conjugated molecular systems. The green and blue isosurface represent the hole and electron density, respectively.

In summary, the reason for the absorption peak red shift, SHG peak shift and sum-frequency ellipse ring shift is due to the charge transfer caused by the different electronegativity of the substituents in the molecular system. However, changes in SHG and sum-frequency coefficients are not significantly related to charge transfer. Because the SHG and sum-frequency coefficients of the carboxyl group and the cyano system are very different but the charge-transfer situation is almost the same, the charge transfer is not the main reason for the change of the nonlinear optical coefficient. On the other hand, different substituents indicate different push–pull functions for electrons. The definition of the second-order nonlinear optical coefficient is:

$$\beta_{ABC}(-\omega_{\sigma}; \omega_1, \omega_2) = \hat{P}[A(-\omega_{\sigma}), B(\omega_1), C(\omega_2)] \sum_{i \neq 0} \sum_{j \neq 0} \frac{\mu_{0i}^A \overline{\mu_{ij}^B} \mu_{j0}^C}{(\Delta_i - \omega_{\sigma})(\Delta_j - \omega_2)} \quad (2)$$

where the $\mu_{ij}^A = \langle i | \hat{\mu}^A | j \rangle$, $\overline{\mu_{ij}^A} = \mu_{ij}^A - \mu_{00}^A \delta_{ij}$, $\omega_{\sigma} = \sum_i \omega_i$ is the transition dipole moment of each excited state, where A, B and C denote one of directions, respectively. The μ_{00}^A is the permanent dipole moment of molecule. The electrostatic properties of different substituents can significantly affect the molecular dipole moment, which can significantly enhance this dipole moment. Therefore, the electrostatic potentials and extreme points of the molecular system with different substituents are shown in Figure 5. It can be seen from the figure that the electrostatic potential distribution of molecules without substituents is very uniform. This uniformly distributed electrostatic potential has a small permanent dipole moment and therefore has a low nonlinear optical coefficient. The substituents of the carboxyl system have the strongest positive electrostatic potential around 51.34 kcal/mol and 53.42 kcal/mol, see Figure 5b. Although the nitro system has a lower electrostatic potential value than the carboxyl system, it has multiple electrostatic potential maximum points, and the conjugated ring in the middle of the molecule constitutes a large intramolecular electric field, see Figure 5d. For the cyano system, although its electrostatic potential value is not small, there are both minimum and maximum values with similar values near the substituent. This can offset the effect of the permanent dipole moment in the nonlinear optical coefficient. Therefore, it can be said that the nitro system constitutes a long-range internal electric field in the molecule and the conjugated ring. However,

carboxyl and cyano systems constitute a small range of intra-molecular electric fields near the substituents. The difference is that the two internal electric fields of the cyano system cancel each other out. This difference in internal electric field is the main reason for the second-order nonlinear optical coefficient changes.

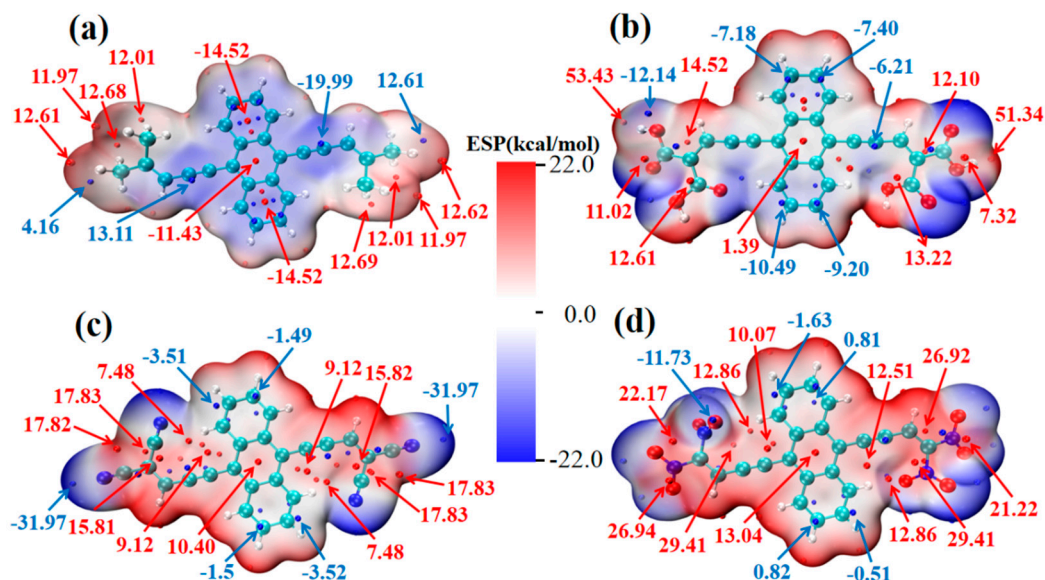


Figure 5. The molecular electrostatic potential vdW isosurface and its extreme points of -H (a), -COOH (b), -CN (c) and -NO₂ (d) conjugated molecular systems. The red and blue regions represent the positive and negative electrostatic potential, respectively.

The above discussion of the transition density matrix (TDM) and electron–hole pair density in S_1 of the molecular system is a qualitative analysis. In order to obtain quantitative information on charge-transfer characteristics of molecular systems. We use the transition index of the wave function to investigate the electronic excitation characteristics. First, the degree of overlap between electrons and holes is defined:

$$S_m(r) = \min[\rho^{hole}(r), \rho^{ele}(r)] \quad (3)$$

$$S_r(r) = \sqrt{\rho^{hole}(r)\rho^{ele}(r)} \quad (4)$$

where $\rho^{hole}(r)$ represents the hole density and $\rho^{ele}(r)$ represents electron density. $S_m(r)$ is the minimum of holes and electrons, $S_r(r)$ is the geometric mean and $S_r(r)$ is greater than $S_m(r)$, which has a better mathematical meaning with better image effect. By plotting these two functions, we can clearly understand which areas have electrons and holes overlapping more significantly.

The quantitative description of the distribution characteristics of these two functions in the whole space is:

$$S_m index = \int S_m(r) dr = \int \min[\rho^{hole}(r), \rho^{ele}(r)] dr \quad (5)$$

$$S_r index = \int S_r(r) dr = \int \sqrt{\rho^{hole}(r)\rho^{ele}(r)} dr \quad (6)$$

The range of the two indexes is [0, 1]; the larger the index, the higher the degree of overlap between holes and electrons. On the contrary, according to the distance between the

centroids of the electron and the hole, the D index, which measures the distance between the centroid of the hole and the electron, is defined:

$$\begin{aligned} D_X &= |X_{ele} - X_{hole}| \\ D_Y &= |Y_{ele} - Y_{hole}| \\ D_Z &= |Z_{ele} - Z_{hole}| \end{aligned} \quad (7)$$

$$D_{index} = \sqrt{(D_X)^2 + (D_Y)^2 + (D_Z)^2} \quad (8)$$

where X_{hole} is the X coordinate of the hole centroid, which can be obtained by multiplying the function by the coordinate variable and integrating in the whole space. In addition to the overall investigation of the hole–electron characteristics, it is also necessary to further investigate the hole–electron density difference, so the σ is defined. The three components, X, Y and Z, are equivalent to the root mean square deviation (RMSD) of the distribution of holes or electrons in the X, Y, Z directions, which reflects the breadth of hole and electron distribution. Where σ for the X component of the hole is defined as:

$$\sigma_{hole,x} = \sqrt{\int (x - X_{hole})^2 \rho^{hole}(r) dr} \quad (9)$$

The transition index of different substituents in S_1 is shown in Table 1. It can be clearly seen that the electron–hole overlap degree of the molecular system with substituents is smaller than that of the molecular system without substituents. Since the D index that measures the distance between the electron–hole centroids of the cyano group and the nitro group has the same value, this charge transfer cannot be regarded as a unidirectional charge-transfer excitation. It is also necessary to consider the difference in the overall spatial distribution of electrons and holes $\Delta\sigma$. It is defined as follows:

$$\begin{aligned} \Delta\sigma_\lambda &= \sigma_{ele,\lambda} - \sigma_{hole,\lambda} \quad \lambda = \{x, y, z\} \\ \Delta\sigma_{index} &= |\sigma_{ele}| - |\sigma_{hole}| \end{aligned} \quad (10)$$

where $\Delta\sigma_\lambda$ is the difference in the spatial distribution of electrons and holes in the direction. The molecular system with substituents is significantly larger than the molecular system without substituents. This is because charge transfer can proceed in multiple directions when electrons are excited, and electron distribution tends to be centrosymmetric, which can be clearly seen on the electron–hole pair density map.

Table 1. Transition indices of molecular systems with different substituents in S_1 .

Substituent	-H	-COOH	-CN	-NO ₂
Excited energy [eV]	2.771	2.424	2.255	2.207
Sm	0.576	0.544	0.501	0.459
Sr	0.876	0.806	0.776	0.749
D [angstrom]	0.005	0.176	0.000	0.000
$\Delta\sigma$	−0.097	0.678	0.773	1.107

3. Materials and Methods

The molecular structure is optimized by using the B3LYP functional [27] in DFT [28] method in combination with the 6–31 G(d) basis set [29] with Gaussian 16 A03 [30]. Using the optimized structure, TDDFT [31] was used to combine the CAM-B3LYP functional [32] and the 6–31 G(d) basis function group for the excited state calculation, and all configuration coefficients were output. The ground-state optimization and excited-state calculations use different functionals. This is because the excited-state calculation uses range-separation functionals to take full account of the remote effects in the charge-transfer process. In the TDDFT calculation, the program first performs a ground state self-consistent field

calculation to determine the ground state. The first hyperpolarizability needs to find the third derivative of the energy E . The DFT method is used to calculate the third-order analytical derivative, and the second-harmonic generation coefficient SHG is obtained by the keyword `polar = DCSHG`. Therefore, the use of different functionals is theoretically necessary and reasonable. Based on this, the Multiwfn program [33] is used for electron-hole analysis, TDM and other electron excitation index and drawing using the VMD program [34].

4. Conclusions

In this work, we calculated the linear and nonlinear optical properties of four different substituents through theoretical calculations. Through the electron-hole pair analysis and the molecular surface electrostatic potential, the physical mechanism between the intra-molecular electric field and nonlinear optical properties was studied. First, the intra-molecular electric field can induce the occurrence of charge transfer to shift the absorption spectrum peak, SHG peak and the radius of the sum-frequency coefficient elliptic ring. Second, the direction and magnitude of the electric field in the molecule will effectively regulate the magnitude of the nonlinear optical coefficient by adjusting the permanent dipole moment. The degree of adjustment is above 10^4 . This conclusion can be applied to nonlinear optical microscopy to distinguish the surface modification of some organic electronic devices and the distribution of different types of substituents.

Author Contributions: Formal analysis, Y.L.; Investigation, L.W.; Methodology, J.W.; Resources, S.C.; Software, D.H.; Writing—original draft, Q.L.; Writing—review & editing, M.W. All authors have read and agreed to the published version of the manuscript.

Funding: This work was supported by the National Nature Science Foundation of China (grant no. 12104202) and project ZR2019PA011 was supported by the Shandong Provincial Natural Science Foundation.

Conflicts of Interest: The authors declare that the research was conducted in the absence of any commercial or financial relationships that could be construed as a potential conflict of interest.

References

1. Dou, C.; Liu, J.; Wang, L. Conjugated polymers containing B←N unit as electron acceptors for all-polymer solar cells. *Sci. China Chem.* **2017**, *60*, 450–459. [[CrossRef](#)]
2. Miao, W.; Wang, L.; Mu, X.; Wang, J. The magical photoelectric and optoelectronic properties of grapheme nanoribbons and their applications. *J. Mater. Chem. C* **2021**, *9*, 13600. [[CrossRef](#)]
3. Kim, D.E.; Baeg, K.J. Reduction Treatment of Molecular-Doped Polymer Semiconductors for High-Performance N-Channel Organic Field-Effect Transistors. *J. Korean Phys. Soc.* **2019**, *75*, 821–826. [[CrossRef](#)]
4. Wendlandt, A.E.; Stahl, S.S. Quinone-catalyzed selective oxidation of organic molecules. *Angew. Chem. Int. Ed.* **2015**, *54*, 14638–14658. [[CrossRef](#)] [[PubMed](#)]
5. Forrest, S.R. The path to ubiquitous and low-cost organic electronic appliances on plastic. *Nature* **2004**, *428*, 911–918. [[CrossRef](#)] [[PubMed](#)]
6. Cao, J.; Lv, X.; Zhang, P.; Chuong, T.T.; Wu, B.; Feng, X.; Shan, C.; Liu, J.; Tang, Y. Plant Sunscreen and Co (II)/(III) Porphyrins for UV-Resistant and Thermally Stable Perovskite Solar Cells: From Natural to Artificial. *Adv. Mater.* **2018**, *30*, 1800568. [[CrossRef](#)] [[PubMed](#)]
7. Feng, X.; Chen, R.; Nan, Z.A.; Lv, X.; Meng, R.; Cao, J.; Tang, Y. Perfection of Perovskite Grain Boundary Passivation by Eu-Porphyrin Complex for Overall-Stable Perovskite Solar Cells. *Adv. Sci.* **2019**, *6*, 1802040. [[CrossRef](#)]
8. Li, X.; Li, C.; Wu, Y.; Cao, J.; Tang, Y. A reaction-and-assembly approach using monoamine zinc porphyrin for highly stable large-area perovskite solar cells. *Sci. China Chem.* **2020**, *63*, 777–784. [[CrossRef](#)]
9. Sharma, K.; Sharma, V.; Sharma, S.S. Dye-sensitized solar cells: Fundamentals and current status. *Nanoscale Res. Lett.* **2018**, *13*, 1–46. [[CrossRef](#)]
10. Huang, Z.S.; Cai, C.; Zang, X.F.; Iqbal, Z.; Zeng, H.; Kuang, D.B.; Wang, L.; Meier, H.; Cao, D. Effect of the linkage location in double branched organic dyes on the photovoltaic performance of DSSCs. *J. Mater. Chem. A* **2015**, *3*, 1333–1344. [[CrossRef](#)]
11. Hara, K.; Sato, T.; Katoh, R.; Furube, A.; Yoshihara, T.; Murai, M.; Kurashige, M.; Ito, S.; Shinpo, A.; Suga, S. Novel conjugated organic dyes for efficient dye-sensitized solar cells. *Adv. Funct. Mater.* **2005**, *15*, 246–252. [[CrossRef](#)]
12. Ko, S.; Choi, H.; Kang, M.S.; Hwang, H.; Ji, H.; Kim, J.; Ko, J.; Kang, Y. Silole-spaced triarylamine derivatives as highly efficient organic sensitizers in dye-sensitized solar cells (DSSCs). *J. Mater. Chem.* **2010**, *20*, 2391–2399. [[CrossRef](#)]

13. Lu, Q.C.; Wang, Q.G.; Song, P.; Ma, F.C.; Yang, Y.; Li, Y. PCDTBT8-doped PffBT4T-2OD-based ternary solar cells with enhanced open-circuit voltage, fill factor and charge separation efficiency. *Solar RRL* **2021**, *10*, 1002. [[CrossRef](#)]
14. Qiao, W.; Yu, H.; Chen, X. Physical mechanism of special type photoinduced charge transfer in one-photon and two-photon absorption of Mobius rings. *Spectrochim. Acta Part A Mol. Biomol. Spectrosc.* **2020**, *236*, 118264. [[CrossRef](#)] [[PubMed](#)]
15. Bo, W.; Zou, Y.; Wang, J. Novel electrical properties and applications in kaleidoscopic graphene nanoribbons. *RSC Adv.* **2021**, *11*, 33675–33691. [[CrossRef](#)]
16. Wang, J.; Mu, X.; Wang, X.; Wang, N.; Ma, F.; Liang, W.; Sun, M. The thermal and thermoelectric properties of in-plane C-BN hybrid structures and graphene/h-BN van der Waals heterostructures. *Mater. Today Phys.* **2018**, *5*, 29–57. [[CrossRef](#)]
17. Wang, J.; Xu, X.; Mu, X.; Ma, F.; Sun, M. Magnetics and spintronics on two-dimensional composite materials of graphene/hexagonal boron nitride. *Mater. Today Phys.* **2017**, *3*, 93–117. [[CrossRef](#)]
18. Wang, J.; Mu, X.; Sun, M.; Mu, T. Optoelectronic properties and applications of graphene-based hybrid nanomaterials and van der Waals heterostructures. *Appl. Mater. Today* **2019**, *16*, 1–20. [[CrossRef](#)]
19. Mu, X.; Wang, J.; Sun, M. Two-dimensional black phosphorus: Physical properties and applications. *Mater. Today Phys.* **2019**, *8*, 92–111. [[CrossRef](#)]
20. Song, J.; Zhang, Z.; Feng, N. Electric Field Induced Twisted Bilayer Graphene Infrared Plasmon Spectrum. *Nanomaterials* **2021**, *11*, 2433. [[CrossRef](#)]
21. Mu, X.; Zong, H.; Zhu, L.; Sun, M. External electric field-dependent photoinduced charge transfer in a donor-acceptor system in two-photon absorption. *J. Phys. Chem. C* **2020**, *124*, 2319–2332. [[CrossRef](#)]
22. Mu, X.; Wang, X.; Quan, J.; Sun, M. Photoinduced Charge Transfer in Donor-Bridge-Acceptor in One-and Two-photon Absorption: Sequential and Superexchange Mechanisms. *J. Phys. Chem. C* **2020**, *124*, 4968–4981. [[CrossRef](#)]
23. Chen, X.; Qiao, W.; Miao, W. The Dependence of implicit Solvent Model parameters and electronic Absorption Spectra and photoinduced charge transfer. *Sci. Rep.* **2020**, *10*, 1–8. [[CrossRef](#)] [[PubMed](#)]
24. Mu, X.; Cai, K.; Wei, W.; Li, Y.; Wang, Z.; Wang, J. Dependence of UV-Visible absorption characteristics on the migration distance and the hyperconjugation effect of a methine chain. *J. Phys. Chem. C* **2018**, *122*, 7831–7837. [[CrossRef](#)]
25. Ding, F.; Kuiken, B.E.; Eichinger, B.E. An efficient method for calculating dynamical hyperpolarizabilities using real-time time-dependent density functional theory. *J. Chem. Phys.* **2013**, *138*, 064104. [[CrossRef](#)]
26. Mu, X.; Wang, J.; Sun, M. Visualization of photoinduced charge transfer and electron-hole coherence in two-photon absorption. *J. Phys. Chem. C* **2019**, *123*, 14132–14143. [[CrossRef](#)]
27. Becke, A.D. Density-functional exchange-energy approximation with correct asymptotic behavior. *Phys. Rev. A* **1988**, *38*, 3098. [[CrossRef](#)] [[PubMed](#)]
28. Stephens, P.; Devlin, F.; Chabalowski, C.; Frisch, M.J. Ab initio calculation of vibrational absorption and circular dichroism spectra using density functional force fields. *J. Phys. Chem.* **1994**, *98*, 11623–11627. [[CrossRef](#)]
29. Petersson, a.; Bennett, A.; Tensfeldt, T.G.; Al-Laham, M.A.; Shirley, W.A.; Mantzaris, J. A complete basis set model chemistry. I. The total energies of closed-shell atoms and hydrides of the first-row elements. *J. Chem. Phys.* **1988**, *89*, 2193–2218. [[CrossRef](#)]
30. Frisch, M.; Trucks, G.; Schlegel, H.; Scuseria, G.; Robb, M.; Cheeseman, J.; Scalmani, G.; Barone, V.; Petersson, G.; Nakatsuji, H. *Gaussian 16, Revision A03*; Gaussian, Inc.: Wallingford, CT, USA, 2016.
31. Furche, F.; Ahlrichs, R. Adiabatic time-dependent density functional methods for excited state properties. *J. Chem. Phys.* **2002**, *117*, 7433–7447. [[CrossRef](#)]
32. Yanai, T.; Tew, D.P.; Handy, N.C. A new hybrid exchange-correlation functional using the Coulomb-attenuating method (CAM-B3LYP). *Chem. Phys. Lett.* **2004**, *393*, 51–57. [[CrossRef](#)]
33. Lu, T.; Chen, F. Multiwfn: A multifunctional wavefunction analyzer. *J. Comput. Chem.* **2012**, *33*, 580–592. [[CrossRef](#)] [[PubMed](#)]
34. Humphrey, W.; Dalke, A.; Schulten, K. VMD: Visual molecular dynamics. *J. Mol. Graph.* **1996**, *14*, 33–38. [[CrossRef](#)]